Enhancement of gaps in thin graphitic films for heterostructure formation

J.P. Hague

The Open University, Walton Hall, Milton Keynes, MK7 6AA, United Kingdom

Abstract.

There are a large number of atomically thin films with similar structure to graphene. These films have a spread of bandgaps relating to their ionicity, and also to the substrate on which they are grown. Such films could have a range of applications in digital electronics where graphene is difficult to use. I use the dynamical cluster approximation to show how electron-phonon coupling between film and substrate can enhance these gaps in a way that depends on the range and strength of the coupling, as well as the length scales of spatial fluctuations. One of the driving factors in this effect is the proximity to a charge density wave instability, which could in principle generate gaps in graphene. The enhancement at intermediate coupling is sufficiently large that spatially varying substrates and superstrates could be used to create heterostructures in thin graphitic films with position dependent electron-phonon coupling and gaps, leading to advanced electronic components.

PACS numbers: 71.45.Lr, 71.38.-k, 73.22.Pr, 73.61.Ey

1. Introduction

The 2D material graphene has made headlines over the past decade for its remarkable properties. Often overlooked is the availability of other two-dimensional graphitic materials which have a similar structure and properties to graphene, but with a direct bandgap that is lacking in suspended graphene. These gapped compounds have the potential to make graphene compatible digital transistors, semiconductor lasers and solar cells. Atomically thick graphitic materials with honeycomb lattices and an inherent direct bandgap formed because of strong ionicity include boron nitride (BN) [1] (band gap $\sim$ 5.6eV [2]) and other materials can be grown in very similar hexagonal Wurtzite layers, such as InN (band gap 0.7-0.8eV) [3], InSb (0.2eV [4], possibly down to 45meV on certain substrates [5]), GaN (2.15eV [6]), and AlN (6.28eV [7]). It has also been reported that small gaps can be formed with a similar mechanism in graphene-gold-ruthenium systems [8] and graphene-SiC systems (there is some debate about the latter [9, 10]).

Recently, I used a self-consistent mean-field theory to show that gaps in atomically thin hexagonal materials may be modified by introducing strong electron-phonon coupling through a highly polarisable superstrate [11, 12]. Similar interactions between graphitic monolayers and substrates form polaronic states and affect the overall electronic structure of the monolayers, as shown by quantum Monte Carlo simulations for highly doped thin graphitic films [13]. Effective electron-electron interactions can be induced via a strong coupling between the electrons in atomically

thick monolayer and phonons in a highly polarisable substrate because of limited out of plane screening, similar to that seen for quasi-2D materials [14]. Such interactions have been experimentally demonstrated between carbon nanotubes and a SiO_2 substrate [15], and are necessary to account for the lower mobilities of graphene on SiO_2 [16].

Here, I make calculations beyond the mean-field theory by using the dynamical cluster approximation (DCA) to compute the effects of electron-phonon interaction on electrons in atomically thick graphitic materials, where a gap has been opened because of ionicity. I present results computed with a high order perturbation theory consistent with Migdal's theorem (which allows neglect of vertex corrections for low phonon frequency and weak coupling) and discuss the effect of long range interactions and spatial fluctuations.

Besides the use of electron-phonon interactions with substrates, the possibility of tuneable gaps has mainly focused on graphene. Following a theoretical proposal [17, 18], bilayer graphene has been observed to have a gap that can be tuned by applying an external electric field [19, 20]. Electron confinement in graphene nanoribbons leads to gaps [21], and high quality nanoribbons can be made by unzipping nanotubes [22] or using patterned SiC steps [23]. Very wide bandgaps can be formed by functionalizing graphene with hydrogen (graphane) [24, 25, 26] and fluorine (fluorographene) [27, 28].

This paper is organised as follows: A model Hamiltonian for the interactions between graphitic monolayers and substrates is introduced in Sec. 2. The perturbative expansion and dynamical cluster formalism used to solve the model are discussed in Sec. 3. Sec. 4 presents details of gap enhancements and the spontaneous formation of a charge density wave state. A summary and conclusions are presented in Sec. 5.

2. Model Hamiltonian

The Hamiltonian required to describe the motion of electrons in thin films with honeycomb lattices has a basis of two atoms. Typically, electron motion within the plane is described using a tight binding model, and ionicity is taken into account with the potential $\pm\Delta$ on the two sublattices. With a highly polarisable substrate, there is additional electron-phonon interaction between the electrons in the film and phonons in the substrate, which may be long range (i.e. momentum dependent). A Hamiltonian with these properties has the form,

$$H = H_{\rm tb} + H_{\rm el-ph} + H_{\rm ph} \tag{1}$$

where $H_{\rm tb}$ is the tight binding Hamiltonian representing the kinetic energy of the electrons in the monolayer, $H_{\rm el-ph}$ describes the electron-phonon interaction, and $H_{\rm ph}$ is the energy of the phonons in the substrate (treated as harmonic oscillators, and including both kinetic and potential energy of the ions).

The tight binding part of the Hamiltonian is written,

$$\begin{aligned} H_{\rm tb} = \sum_{\boldsymbol{k}\sigma} (&\phi_{\boldsymbol{k}} a^\dagger_{\boldsymbol{k}\sigma} c_{\boldsymbol{k}\sigma} + \phi^*_{\boldsymbol{k}} c^\dagger_{\boldsymbol{k}\sigma} a_{\boldsymbol{k}\sigma} \\ &+ \Delta(a^\dagger_{\boldsymbol{k}\sigma} a_{\boldsymbol{k}\sigma} - c^\dagger_{\boldsymbol{k}\sigma} c_{\boldsymbol{k}\sigma})). \end{aligned} \tag{2}$$

The first part represents the kinetic energy, where $\phi_{\boldsymbol{k}} = -t\sum_i \exp(i\boldsymbol{k}.\boldsymbol{\delta}_i)$ and $\boldsymbol{\delta}_i$ are the nearest neighbour vectors from A to B sub-lattices, $\boldsymbol{\delta}_1 = \tilde{a}(1, \sqrt{3})/2$, $\boldsymbol{\delta}_2 = \tilde{a}(1, -\sqrt{3})/2$ and $\boldsymbol{\delta}_3 = (-\tilde{a}, 0)$ and $\tilde{a}$ is the spacing between carbon atoms in the plane (the tilde is used to avoid confusion with the creation and annihilation

operators). Electrons with momentum $\boldsymbol{k}$ are created on A sites with the operator $a^\dagger_{\boldsymbol{k}}$ and B sites with $c^\dagger_{\boldsymbol{k}}$. The second part represents the interaction between electrons in the monolayer and a static potential, either induced by the substrate (in the case of graphene) or by ionicity (in monolayers of III-V semiconductors). Here, A sites have a higher potential, Δ and B sites are lower in energy by $-\Delta$. Breaking the symmetry between A and B sites in the bipartite honeycomb lattice gives rise to a gap.

The phonon part of the Hamiltonian is,

$$H_{\rm ph} = \sum_{\boldsymbol{q}} \Omega_{\boldsymbol{q}} (b^\dagger_{\boldsymbol{q}} b_{\boldsymbol{q}} + d^\dagger_{\boldsymbol{q}} d_{\boldsymbol{q}}) \tag{3}$$

where phonons with momentum $\boldsymbol{q}$ are created on A and B sites with $b^\dagger_{\boldsymbol{q}}$ and $d^\dagger_{\boldsymbol{q}}$ respectively. Typically, the phonon dispersion, $\Omega_{\boldsymbol{q}}$ is taken to be momentum independent as a good approximation to optical phonons. Typical phonon frequencies vary from 10s to 100s of meV. For example, in BN phonon energies range from 110meV for transverse acoustic phonons at the K point to 200meV for optical phonons [29]. Due to ionicity, sites have a net charge, so strong coupling between electrons and phonons is expected.

Finally, the interaction between electrons in the monolayer and phonons in the substrate (or superstrate in the case of graphene on a substrate) is,

$$\begin{aligned} H_{\rm el-ph} = &\sum_{\boldsymbol{kq}} g_{\boldsymbol{q}} \left[c^\dagger_{\boldsymbol{k-q}} c_{\boldsymbol{k}} (d^\dagger_{\boldsymbol{q}} + d_{\boldsymbol{-q}}) + a^\dagger_{\boldsymbol{k-q}} a_{\boldsymbol{k}} (b^\dagger_{\boldsymbol{q}} + b_{\boldsymbol{-q}}) \right] \\ &+ \sum_{\boldsymbol{kq}} \tilde{g}_{\boldsymbol{q}} \left[a^\dagger_{\boldsymbol{k-q}} a_{\boldsymbol{k}} (d^\dagger_{\boldsymbol{q}} + d_{\boldsymbol{-q}}) + c^\dagger_{\boldsymbol{k-q}} c_{\boldsymbol{k}} (b^\dagger_{\boldsymbol{q}} + b_{\boldsymbol{-q}}) \right] \end{aligned} \tag{4}$$

where the coupling constants g and $\tilde{g}$ represent interactions between electrons and phonons on the same sub-lattice and different sub-lattices respectively. A lattice Fröhlich electron-phonon interaction with the form,

$$g_{\boldsymbol{m}}(\boldsymbol{n}) \propto \exp(-|\boldsymbol{n}-\boldsymbol{m}|/R_{sc})[(\boldsymbol{n}-\boldsymbol{m})^2 + \tilde{c}^2]^{-3/2}, \tag{5}$$

has been proposed for layered quasi-2D systems [14]. Experiment has demonstrated that this form explains interactions between electrons in carbon nanotubes placed on SiO_2 [15], and is necessary to account for reduced mobilities when graphene is placed on a substrate [16]. The screening radius, R_{sc} controls the length scale of the interaction. $\tilde{c}$ is the distance between the graphitic thin film and surface atoms in the substrate. In the following, I take $\tilde{c}^2 = 2\tilde{a}^2$, since the distance between graphene and substrate (which are typically bound by van der Walls interactions) is likely to be slightly larger than between the very strongly bound carbon atoms in the graphene layer. Ionic, graphitic materials may bind more strongly to appropriate ionic substrates leading to shorter $\tilde{c}$, which in this work is represented (in combination with screening effects) with a reduced R_{sc}. In practice, the effects of changing $\tilde{c}$ and R_{sc} on the form of the effective electron-electron coupling mediated by phonons are very similar.

The model used here has some similarities to the ionic Hubbard model [30]. In the ionic Hubbard model, the ionicity (introduced by an analogous parameter Δ) acts against the Mott insulating state (which is caused by the repulsive Hubbard U). In contrast, in the model here, the parameter Δ acts with the electron-phonon coupling to form a charge density wave (CDW) insulating (gapped) state.

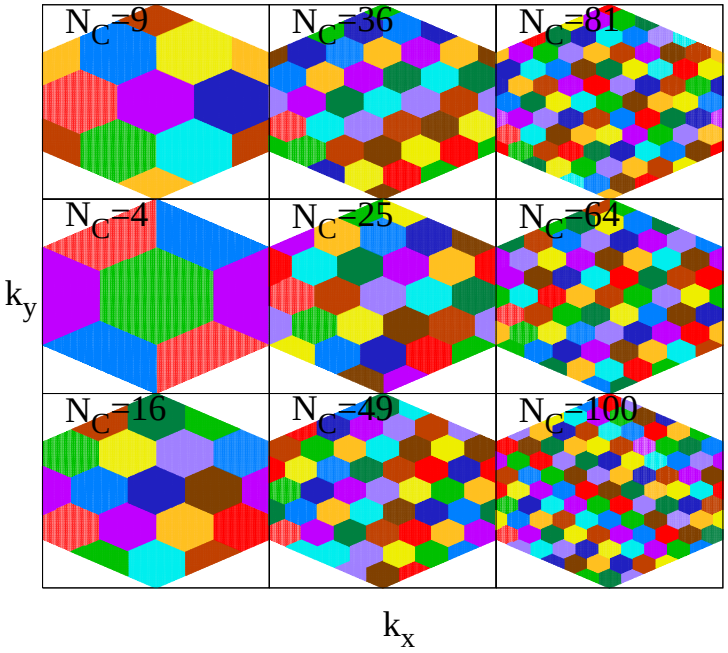

Figure 1. (Colour online) Dynamical cluster approximation (DCA) sub-zones for cluster sizes of up to $N_C = 100$. Within each sub-zone, the self-energy is taken to be momentum independent. This allows Green functions to be calculated in the thermodynamic limit, and convergence properties are particularly good as N_C is increased. Note that the only symmetry taken into account is translation in $\boldsymbol{k}$-space.

3. Method

The electron-phonon Hamiltonian described above is extremely difficult to solve exactly using numerical methods. An approximate solution can be made using perturbation theory within the dynamical cluster approximation formalism. The dynamical cluster approximation (DCA) [31, 32] is one of the possible ways of extending dynamical field theory ‡ (DMFT)[33] so that it can be applied accurately to low dimensional systems. The Mermin-Wagner-Hohenberg theorem indicates that the significant non-local fluctuations found in one- and two- dimensions are expected to eliminate spontaneous long range order, potentially rendering results from mean-field theories qualitatively wrong [34, 35]. DCA resolves this problem by re-introducing spatial fluctuations.

When applying DCA, the Brillouin zone is divided up into N_C sub-zones centred about a momentum vector $\boldsymbol{K}_i$ (see Fig. 1) consistent with the symmetry of the whole system. Within each sub-zone, the self-energy is approximated as a momentum-independent function, so the Green function can be coarse grained by integrating over the sub-zone,

$$\mathbf{G}(\boldsymbol{K}_\mathrm{i}, \mathrm{z}) = \sum_{\boldsymbol{k} \in \boldsymbol{K}_i} [\mathbf{I}(\mathrm{z} + \mu) + \Delta \boldsymbol{\sigma}_3 - \boldsymbol{\Phi}_{\boldsymbol{k}} - \boldsymbol{\Sigma}(\boldsymbol{K}_\mathrm{i}, \mathrm{z})]^{-1}. \tag{6}$$

‡ Where DMFT is used to approximate low dimensional systems, it is often known as the local approximation

$$\equiv \begin{bmatrix} G_{AA} & G_{AB} \\ G_{BA} & G_{BB} \end{bmatrix} \tag{7}$$

where A and B represent sublattices and

$$\boldsymbol{\Phi}_{\boldsymbol{k}} = \begin{bmatrix} 0 & \phi_{\boldsymbol{k}} \\ \phi^*_{\boldsymbol{k}} & 0 \end{bmatrix}, \boldsymbol{\sigma}_3 = \begin{bmatrix} 1 & 0 \\ 0 & -1 \end{bmatrix} \tag{8}$$

In finite size techniques, the number of particles is related to the number of momentum points used in the calculation of the self energy. In contrast, the DCA coarse-graining step involves an infinite number of momentum points, so the thermodynamic limit is satisfied for any cluster size. In the context of the perturbation theory for the Migdal–Eliashberg theory used here, DCA has particularly good convergence properties in cluster size N_C, so in principle smaller clusters can be used leading to a significant improvement in computational efficiency [36, 37].

In several previous studies, $N_C = 4$ and $N_C = 16$ DCA clusters have been used to understand Hubbard interactions on hexagonal/triangular lattices (see e.g. [38]). I briefly discuss the subzone schemes for hexagonal lattices with larger N_C. For the lattices used here, the simplest way of defining the sub-zone vectors is: $\tilde{\boldsymbol{k}}_1 = \boldsymbol{k}_1/\sqrt{N_C}$, $\tilde{\boldsymbol{k}}_2 = \boldsymbol{k}_2/\sqrt{N_C}$ with the vectors $\boldsymbol{K}_i = n\tilde{\boldsymbol{k}}_1 + m\tilde{\boldsymbol{k}}_2$ with n and m integers. Here, the reciprocal lattice vectors are $\boldsymbol{k}_1 = (2\pi/3\tilde{a}, 2\pi/\sqrt{3}\tilde{a})$ and $\boldsymbol{k}_2 = (2\pi/3\tilde{a}, -2\pi/\sqrt{3}\tilde{a})$. There are likely to be other valid lattices that can also be used, where the lattice and sub-lattice are oriented at different angles. However, the lattices used there are the simplest to implement.

Even for the simple cases considered here, the resultant lattices can be ordered into groups. Clusters with $N_C = (3n)^2$ ($N_C = 9$, $N_C = 36$, $N_C = 81$ etc.) have sub-zones centred on the K and K′ points (here $n \geq 1$ is an integer). Those with $N_c = (3n-1)^2$ ($N_C = 4$, $N_C = 25$ and $N_c = 64$) make a second set where 3 sub-zones share a corner at the K and K′ points, and the third set of $N_c = (3n+1)^2$ ($N_C = 16, 64, 100$ etc.) where 3 sub-zones share a corner at the K and K′ points and an edge with the full Brillouin zone. Since the self energies would be identical in the 3 zones around the K and K′ points in the latter 2 cases, they will poorly describe the physics at the K and K′ points (which is especially important for graphene). This is why I use only the $(3n)^2$ series.

To establish which $\boldsymbol{k}$ point belongs to a sub zone, it is sufficient to find the closest $\boldsymbol{K}_i$ point corresponding to the centre of the sub-zone (subject to shifts of reciprocal lattice vectors). The edges of the shapes defined in this way are the hexagons in the figure.

The perturbation theory used here can be seen in Fig. 2. Panel (a) shows the Hartree diagram. For the symmetry broken states, this cannot be absorbed into the chemical potential, and is the main contributor to modification of the gap. The Fock potential (shown in panel (b)) is responsible for frequency dependence of the self-energy. Phonon propagators are modified using a Dyson equation (panel (c)) which modifies the phonon frequency, and can lead to further enhancement of the band gap. Therefore,

$$\Sigma^{(H)}_{ij} = -2\frac{T}{N_C}\delta_{ij}\sum_{lm\boldsymbol{K}'} D_{il}(\boldsymbol{0})G_{ll}(\boldsymbol{K}', \omega_m) \tag{9}$$

$$\Sigma^{(F)}_{ij}(\omega_n\boldsymbol{K}) = \frac{T}{N_C}\sum_{\omega_s,\boldsymbol{Q}} G_{ij}(\omega_n - \omega_s, \boldsymbol{K} - \boldsymbol{Q})D_{ij}(\omega_s\boldsymbol{Q}) \tag{10}$$

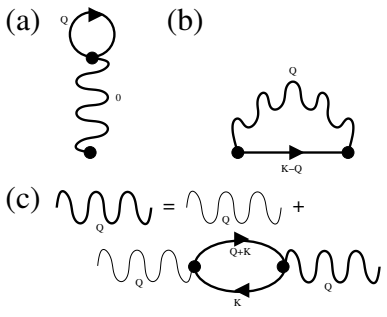

Figure 2. Perturbation theory used in the work presented here. (a) Hartree diagram. For the symmetry broken states, this cannot be absorbed into the chemical potential, and is the main contributor to modification of the gap (b) The Fock potential is responsible for frequency dependence of the self-energy (c) Dyson equation for the phonon propagator. This renormalizes the phonon frequency, which can lead to further enhancement of the band gap.

where $\boldsymbol{Q}$ represent the centres of the coarse-grained cells for phonon momenta.

$$D_{ij}^{-1}(\boldsymbol{Q}) = d_{ij}^{-1}(\boldsymbol{Q}) - \Pi_{ij}(\boldsymbol{Q}) \tag{11}$$

where

$$\Pi_{ij}(\boldsymbol{Q}, \omega_s) = -2\frac{T}{N_C}\sum_{\boldsymbol{K}\omega_n} G_{ij}(\boldsymbol{Q}+\boldsymbol{K}, \omega_n+\omega_s)G_{ji}(\boldsymbol{K}, \omega_n) \tag{12}$$

and the non-interacting phonon propagator is,

$$d_{ij}(\boldsymbol{Q}, \omega_s) = \lambda_{ij}(\boldsymbol{Q})\Omega^2/(\Omega^2+\omega_s^2). \tag{13}$$

Here the dimensionless, momentum dependent electron-phonon coupling is defined using the following procedure. First, the coupling for a single $\boldsymbol{k}$ value is defined to be $\tilde{\lambda}_{\boldsymbol{k}}^{(ij)} = |f_{\boldsymbol{k}}^{(ij)}|^2/2Mt\Omega^2$ where $f_{\boldsymbol{k}}^{(AA)} = f_{\boldsymbol{k}}^{(BB)} = \sum_i e^{i\boldsymbol{k}\cdot\boldsymbol{R}_i} f_{\boldsymbol{R}_i}$, $f_{\boldsymbol{k}}^{(AB)} = \sum_i e^{i\boldsymbol{k}\cdot\boldsymbol{R}_i + i\tilde{a}} f_{\boldsymbol{R}_i+i\tilde{a}}$ and $f_{\boldsymbol{k}}^{(BA)} = \sum_i e^{i\boldsymbol{k}\cdot\boldsymbol{R}_i - i\tilde{a}} f_{\boldsymbol{R}_i-i\tilde{a}}$. Here, $f_{\boldsymbol{R}_i} = g_{\boldsymbol{0}}(\boldsymbol{R}_i)\sqrt{2M\Omega/\hbar}$, the lattice vectors are $\boldsymbol{R}_i = \tilde{n}\boldsymbol{a}_1 + \tilde{m}\boldsymbol{a}_2$, $\boldsymbol{a}_1 = 3\boldsymbol{i}/2 + \sqrt{3}\boldsymbol{j}/2$ and $\boldsymbol{a}_2 = 3\boldsymbol{i}/2 - \sqrt{3}\boldsymbol{j}/2$.

The dimensionless electron-phonon coupling can then be related to $\lambda_{ij}(\boldsymbol{Q})$ via,

$$\lambda_{ij}(\boldsymbol{K}_i) = 2N_C\lambda\frac{\sum_{\boldsymbol{k}\in\boldsymbol{K}_i}\tilde{\lambda}_{\boldsymbol{k}}^{(ij)}}{\sum_{\boldsymbol{k}'\in BZ, nm}\tilde{\lambda}_{\boldsymbol{k}'}^{(nm)}} \tag{14}$$

4. Results

The aim of the work presented here is to use dynamical cluster approximation (DCA) to examine how charge density wave (CDW) gaps in graphitic thin films vary with electron-phonon coupling. I take $T = 0.02t$, $\Delta = 0.1t$ and $\Omega = 0.01t$. Noting that t is typically on the order of an eV, these values correspond approximately to room temperature, phonon frequencies, Ω, of 10s of meV and Δ a few hundred meV, consistent with thin films of materials such as InSb, or reported gaps in some graphene on substrate systems.

I start by computing self-energies to show the relative contributions of on- and off-site terms, and the effects of varying the interaction range. The computed self energies, including the relative contributions of Hartree and Fock diagrams for $\lambda = 2$ and

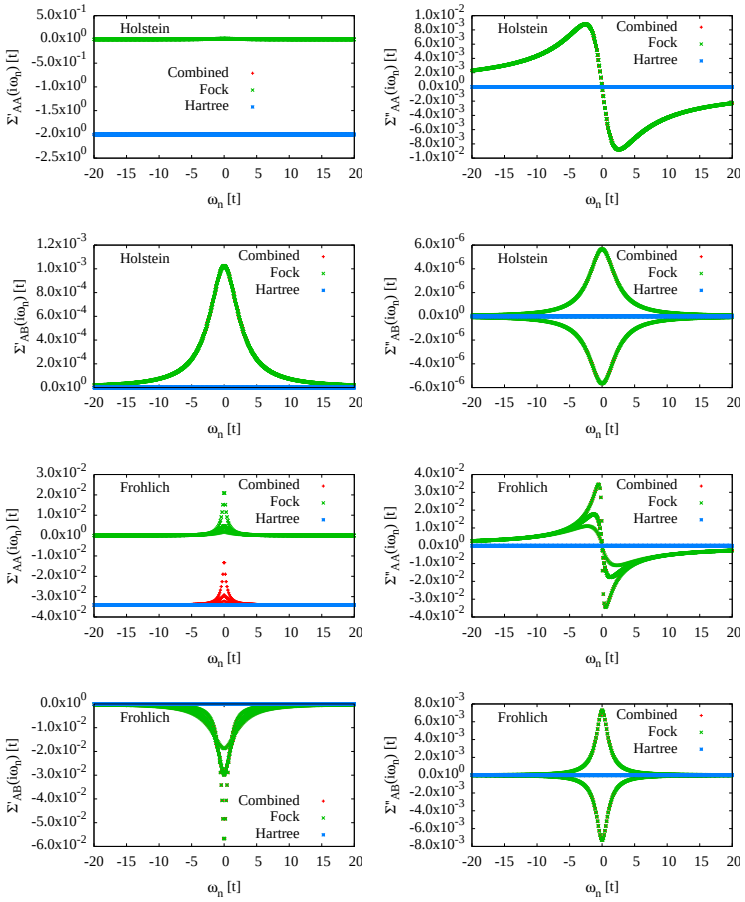

Figure 3. (color online) Comparison of Hartree and Fock parts of self energy, $\Sigma = \Sigma' + i\Sigma''$. The main contribution to the self energy is the real part of the Hartree term, which is momentum independent. N.B. The Fock term is still the most important contribution in some cases, for example the inverse mass depends on derivatives of the self energy, so this will be given by the Fock term. $T = 0.02t$, $\Delta = 0.1t$, $\Omega = 0.01t$, $\lambda = 2$ and $N_C = 9$.

$N_C = 9$ are shown in Fig. 3. The real part of the Hartree diagram is momentum and energy independent. It is the largest part of the self energy, and directly contributes to the enhancement to the gap, and also is the main contributor to spontaneous CDW order. N.B. The Fock term is still the most important contribution for some properties, for example the inverse mass (not considered here) depends on derivatives of the self energy, so this property will be given by the Fock term. The real parts of the on-site self energies are significantly smaller for the long-range Fröhlich interaction than for the Holstein model. Other differences are that the off-site self energy is small for the Holstein interaction (N.B. it is not zero because of effective off-site interactions mediated through the phonon self-energy), whereas it is of similar magnitude to (but smaller than) the onsite self-energy for the Fröhlich interaction.

The main aim of this paper is to understand the role of electron-phonon coupling range in the enhancement of gaps. Figure 4 shows how the enhancement varies with

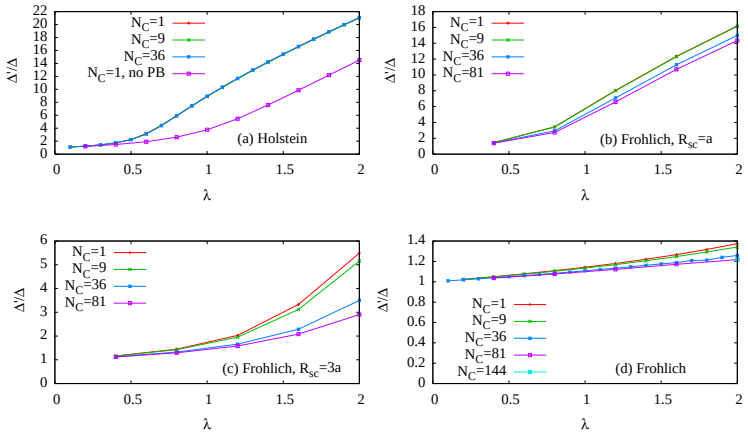

Figure 4. (color online) (a) Gap enhancement for a Holstein interaction with $\Delta/t = 0.1$, comparing results from the dynamical mean-field theory and DCA. There are only small corrections due to momentum dependence. (b) Gap enhancement for the long range Fröhlich interaction, $R_{sc} = 1$ (c) Gap enhancement for the long range Fröhlich interaction, $R_{sc} = 3$ (d) Gap enhancement for the long range Fröhlich interaction. The $N_C = 144$ point at $\lambda = 2$ in panel (d) demonstrates that convergence has been achieved. Here $T = 0.02t$ and $\Omega = 0.01t$.

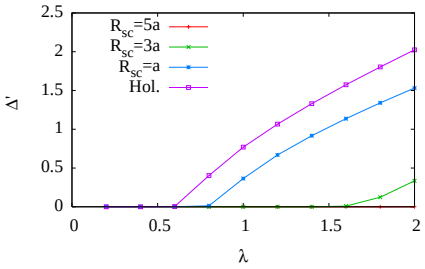

Figure 5. (color online) Spontaneous symmetry breaking. Here $T = 0.02t$, $\Omega = 0.01t$, $N_C = 1$ and $\Delta = 0$. Note that a larger λ value is required to see CDW for longer range interactions, but the effect is still present.

interaction range and with cluster size. Larger cluster size means longer range spatial fluctuations with length scale $\sim \sqrt{N_C}$. Figure 4(a) shows gap enhancement for a Holstein interaction with $\Delta/t = 0.1$, comparing results from the dynamical mean-field theory and DCA. N.B. The enhancements will be smaller for systems with large ionicity [11, 12]. There are very small corrections due to momentum dependence. As the screening radius, R_{sc} increases, the enhancement decreases. Spatial fluctuations have no effect on this set of diagrams for the Holstein interaction. Figs. 4(b) and 4(c) show results when $R_{sc} = 1$ and $R_{sc} = 3$ respectively. Essentially, the effective λ decreases with R_{sc}. This is most extreme for $R_{sc} \to \infty$ and Fig. 4(d) shows gap enhancement for the long range Fröhlich interaction. The reductions in gap enhancement due to spatial fluctuations are also most pronounced for long range coupling. Convergence is found for $N_C \sim 81$ indicating that spatial fluctuations extend over approximately 9 sites. Clearly the key to finding a strong effect is to reduce the

effective range of the interaction, or alternatively to increase λ. This may be achieved by choosing substrates that sit closer to the graphene, or increasing screening from the substrate.

The phonon self-energy plays an important role in the gap enhancement. Fig 4(a) also shows the enhancement effect when $N_C = 1$ if the polarisation bubble (PB) is neglected and the curve can be compared with the full theory with $N_C = 1$. The phonon self energy augments the enhancement by increasing the value of the phonon propagator at the Brillouin zone centre. Thus, increasing the electron self-energy, which is proportional to the phonon propagator.

It is also interesting to determine if gaps can spontaneously form from the electron-phonon interaction. This is explored in Fig. 5, which shows spontaneous charge density wave (CDW) symmetry breaking when $N_C = 1$. For sufficient λ, a CDW state can be found for all values of R_{sc} (this is not visible in the figure for large values of R_{sc} because λ values are too small). While it is expected that the CDW state will become more difficult to form as cluster size increases (owing to the Mermin-Wagner-Hohenberg theorem [34, 35]) the result shows that the full system with $\Delta \neq 0$ is on the cusp of a CDW state, and this is why the gap is strongly sensitive to the electron-phonon coupling.

5. Summary and conclusions

In summary, I have investigated gap formation and enhancement in a model of atomically thin graphitic materials. Electron-phonon coupling and range has been varied, and the effects of higher order corrections to the phonon propagator have been considered. The effect of reintroducing fluctuations around the mean field limit has also been investigated using the dynamical cluster approximation. Higher order corrections to the perturbation theory increase the gap enhancement. It is found that gaps are enhanced by electron-phonon interactions for all interaction ranges, with the enhancement decreasing as interaction range increases. The re-introduction of short range fluctuations is also found to cause further decreases to the enhancement. In order to see these effects in real materials, it would be necessary to reduce the range of the interaction, either by choosing ionic substrates that sit close to the graphitic monolayer and have a strong coupling with electrons in the film, or by promoting a strong screening.

One of the driving factors of this enhancement is the proximity to a charge density wave state for a material without ionicity ($\Delta = 0$) such as graphene. I have shown that sufficiently large coupling between electrons and phonons can lead to spontaneous CDW order in the mean-field solution. This instability to order shows why there are significant gap enhancements at large coupling when ionicity is introduced. While a spontaneous CDW state would be unstable in a pure 2D material because of the Mermin-Wagner-Hohenberg theorem [34, 35], a quasi-2D material with weak hopping between layers should be able to generate a CDW state at the temperature characterised by the interplane hopping. Only small interplane hopping due to tunnelling is necessary to stabilise the CDW state (to stabilise a state below $T \sim 500K$, inter plane hopping on the order of 50meV, or around 1% of the in plane hopping is required). Owing to the spontaneous symmetry breaking, an appropriately layered heterostructure of graphene and a wide gap insulating material such as BN might be expected to generate small spontaneous gaps of useful size due to CDW formation.

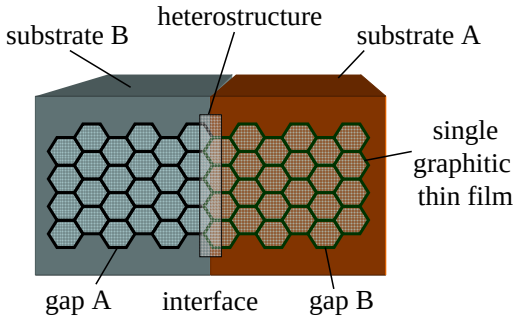

Figure 6. Schematic showing the possible use of two substrates with different electron-phonon coupling to thin graphitic films to make a heterostructure in a single thin film of a graphitic material. This could be manufactured by laying down an interface between the two substrate materials before cleaving perpendicular to the interface and then depositing the thin film.

The results here suggest that an interesting possibility would be to use the electron-phonon interaction to make position dependent changes to the bandstructure of the thin film (for example by adding a spatially dependent superstrate with phonons that strongly couple to electrons in the thin film), a method that is potentially easier to control than trying to deposit neighbouring thin films with interfaces in the plane. The proportional gap enhancements predicted here are similar to those between GaAs and AlGaAs [39], so it is plausible that thin film heterostructures or quantum dots could be built up in this way (see Fig. 6). Another possibility would be to tune inherent gaps in III-V semiconductors with the electron-phonon interaction, so that they become optimal for applications such as solar cells where the efficiency is highly sensitive to the gap size. Clearly graphitic thin films warrant further study to assess their full capability for novel electronics.

Acknowledgments

I am pleased to acknowledge EPSRC grant EP/H015655/1 for funding and useful discussions with Anthony Davenport and Adelina Ilie.

[1] K.S. Novoselov, D. Jiang, F. Schedin, T. J. Booth, V. V. Khotkevich, S. V. Morozov, and A. K. Geim. *PNAS*, 102:10453, 2005.
[2] L. Song, L. Ci, H. Lu, P.B. Sorokin, C. Jin, J. Ni, A.G. Kvashnin, D.G. Kvashnin, J. Lou, B.I. Yakobson, and P.M. Ajayan. *Nano Lett.*, 10:3209, 2010.
[3] J. Wu, W. Walukiewicz, K.M. Yu, J.W. Ager, E.E. Haller, H. Lu, W.J. Schaff, Y. Saito, and Y. Nanishi. *App. Phys. Lett.*, 80:3967, 2002.
[4] I.H. Khan. *Surface Science*, 9:306, 1968.
[5] R.K. Bedi and S. Kaur T. Singh. *Thin Solid Films*, 298:47, 1997.
[6] J. Petalas, S. Logothetidis, S. Boultadakis, M. Alouani, and J.M. Wills. *Phys. Rev. B*, 52:8082, 1995.
[7] F. Litimein, B. Bouhafs, Z. Dridi, and P. Ruterana. *New J. Phys.*, 4:64, 2002.
[8] C. Enderlein, Y. S. Kim, A. Bostwick, E. Rotenberg, and K. Horn. *New J. Phys.*, 12:033014, 2010.

[9] S. Y. Zhou, G.-H. Gweon, A. V. Fedorov, P. N. First, W. A. De Heer, D.-H. Lee, F. Guinea, A. H. Castro Neto, and A. Lanzara. *Nature Materials*, 6:770, 2007.
[10] A. Bostwick, T. Ohta, T. Seyller, K. Horn, and E. Rotenberg. *Nature Physics*, 3:36, 2007.
[11] J. P. Hague. *Phys. Rev. B*, 84:155438, 2011.
[12] J. P. Hague. *Nanoscale research letters*, 7:303, 2012.
[13] J.P. Hague. *Phys. Rev. B*, 86:064302, 2012.
[14] A. S. Alexandrov and P. E. Kornilovitch. *J. Phys.: Condens. Matter*, 14:5337, 2002.
[15] M. Steiner, M. Freitag, V. Perebeinos, J. C. Tsang, J. P. Small, M. Kinoshita, D. Yuan, J. Liu, and P. Avouris. *Nature Nanotechnology*, 4:320, 2009.
[16] S. Fratini and F. Guinea. *Phys. Rev. B*, 77:195415, 2008.
[17] E. McCann and V. I. Falko. *Phys. Rev. Lett.*, 96:086805, 2006.
[18] E. McCann, D. S. L. Abergel, and V. I. Falko. *Solid State Communications*, 143:110, 2007.
[19] T. Ohta, A. Bostwick, T. Seyller, K. Horn, and E. Rotenberg. *Science*, 313:951, 2006.
[20] Y. Zhang, T-T. Tang, C. Girit, Z. Hao, M. C. Martin, A. Zettl, M. F. Crommie, Y. R. Shen, and F. Wang. *Nature*, 459:820, 2009.
[21] M. Y. Han, B. Özyilmaz, Y. Zhang, and P. Kim. *Phys. Rev. Lett.*, 98:206805, 2007.
[22] D. V. Kosynkin, A. L. Higginbotham, A. Sinitskii, J. R. Lomeda, A. Dimiev, B. K. Price, and J. M. Tour. *Nature*, 458:872, 2009.
[23] J. Hicks, A. Tejeda, A. Taleb-Ibrahimi, M. S. Nevius, F. Wang, K. Shepperd, J. Palmer, F. Bertran, P. Le Fvre, J. Kunc, W. A. de Heer, C. Berger, and E. H. Conrad. *Nat. Phys.*, 9:49, 2012.
[24] Jorge O. Sofo, Ajay S. Chaudhari, and Greg D. Barber. Graphane: A two-dimensional hydrocarbon. *Phys. Rev. B*, 75:153401, Apr 2007.
[25] D. W. Boukhvalov, M. I. Katsnelson, and A. I. lichtenstein. *Phys. Rev. B*, 77:035427, 2008.
[26] D. C. Elias, R. R. Nair, T. M. G. Mohiuddin, S. V. Morozov, P. Blake, M. P. Halsall, A. C. Ferrari, D. W. Boukhvalov, M. I. Katsnelson, A. K. Geim, and K. S. Novoselov. *Science*, 323:610, 2009.
[27] J.-C. Charlier, X. Gonze, and J.-P. Michenaud. First-principles study of graphite monofluoride $(cf)_n$. *Phys. Rev. B*, 47:16162–16168, Jun 1993.
[28] S.-H. Cheng, K. Zou, F. Okino, H. R. Gutierrez, A. Gupta, N. Shen, P. C. Eklund, J. O. Sofo, and J. Zhu. Reversible fluorination of graphene: Evidence of a two-dimensional wide bandgap semiconductor. *Phys. Rev. B*, 81:205435, May 2010.
[29] J. Serrano, A. Bosak, R. Arenal, M. Krisch, K. Watanabe, T. Taniguchi, H. Kanda, A. Rubio, and L. Wirtz. *Phys. Rev. Lett.*, 98:095503, 2007.
[30] N. Nagaosa and J. Takimoto. *J. Phys. Soc. Jpn.*, 55:2735, 1986.
[31] M. Hettler, A.N. Tahvildar-Zadeh, M. Jarrell, Th. Pruschke, and H.R. Krishnamurthy. *Phys. Rev. B*, 58:7475, 1998.
[32] M. Hettler, M. Mukherjee, M. Jarrell, and H.R. Krishnamurthy. *Phys. Rev. B*, 61:12739, 2000.
[33] A. Georges, G. Kotliar, W. Krauth, and M. Rozenburg M. *Rev. Mod. Phys*, 68:13, 1996.
[34] N.D. Mermin and H. Wagner. *Phys. Rev. Lett.*, 17:1133, 1966.
[35] P.C. Hohenberg. *Phys. Rev.*, 158:383, 1967.
[36] J.P. Hague. *J. Phys.: Condens. Matter*, 15:2535, 2003.
[37] J.P. Hague. *J. Phys.: Condens. Matter*, 17:5663, 2005.
[38] H. Lee, G. Li, and H. Monien. *Phys. Rev. B*, 78:205117, 2008.
[39] Tsuneya Ando, Alan B. Fowler, and Frank Stern. *Rev. Mod. Phys.*, 54:437, 1982.